Relationship of Iron Deposition to Calcium Deposition in Human Aortic Valve Leaflets

Marion Morvan, Dimitri Arangalage, Grégory Franck, Fanny Perez, Léa Cattan-Levy, Isabelle Codogno, Marie-Paule Jacob-Lenet, Catherine Deschildre, Christine Choqueux, Guillaume Even, et al.

Relationship of Iron Deposition to Calcium Deposition in Human Aortic Valve Leaflets

Marion Morvan [a, *], BSc, Dimitri Arangalage [a, b, c, *], MD, PhD, Grégory Franck [a, *], PhD, Fanny Perez [a], MD, Léa Cattan-Levy [a, b], MD, Isabelle Codogno [b], BSc, Marie-Paule Jacob-Lenet [a], PhD, Catherine Deschildre [a], BSc, Christine Choqueux [a], BSc, Guillaume Even [a], BSc, Jean-Baptiste Michel [a], MD, PhD, Magnus Bäck [d], MD, PhD, David Messika-Zeitoun [a, b, c], MD, PhD, Antonino Nicoletti [a, c], PhD, Giuseppina Caligiuri [a, b, **], MD, PhD, Jamila Laschet [a, c, **]PhD

[a]Institut National de la Santé et de la Recherche Médicale U1148, Paris, France; [b]Department of Cardiology, Bichat Hospital, Paris, France; [c] Université Paris Diderot, Sorbonne Paris Cité, Faculté de Médecine Paris-Diderot, Paris, France; [d]Department of Cardiology, Karolinska University Hospital, Stockholm, Sweden.
* and **: These authors contributed equally to this work, respectively, as * first and **last authors.

Short Title: Intraleaflet hematoma promotes aortic valve calcification

Conflicts: The authors declare that they have no conflicts of interest related to this work.
Funding :
-Fondation de France" (FDF 2008-002724), Paris, France (FDF);
-The French Government, managed by the National Research Agency (ANR) under the "Program Investissements d'Avenir" with the reference ANR-16-RHUS-0003_STOP-AS
-The GENERAC (NCT00647088) study was supported by grants from the Assistance Publique - Hôpitaux de Paris (PHRC National 2005 and 2010, and PHRC regional 2007)
-GF was the recipient of research grants by the Fondation Lefoulon-Delalande, Paris, France; and by the European Union PRESTIGE programme (2017-1-0032).
Acknowledgments: The authors greatly acknowledge Samira Benadda of the CRI U1149 Imaging Facility for her technical assistance.

Address for correspondence
Jamila Laschet, PhD
INSERM U 1148, Bichat Hospital
46 rue Henri Huchard
75018 Paris, France
Telephone: +33 1 40257557, + 33 1 40257558
Fax: +33 1 40258602
E-mail: jamila.laschet@inserm.fr
Twitter: @Inserm

Giuseppina Caligiuri
INSERM U 1148, Bichat Hospital
46 rue Henri Huchard
75018 Paris, France
Telephone: +33 1 40257557 and + 33 1 40257558.
Fax: +33 1 40258602
E-mail: giuseppina.caligiuri@inserm.fr

ABSTRACT
Background: Intraleaflet hematomas are associated with advanced stages of aortic valve calcification and suspected to be involved in disease progression. However, the mechanism by which the entry of blood cells into the valves affects the biology of aortic valvular interstitial cells (VIC) remains to be elucidated.
Objective: To evaluate the putative link between intraleaflet hematoma and aortic valve calcification and to assess its pathophysiological implications.
Methods: The spatial relationship between calcium deposits and intraleaflet hematomas was analyzed by whole-mount staining of calcified and non-calcified human aortic valves, obtained in the context of heart transplantation and from patients who underwent surgical valve replacement. Endothelial micro-fissuring was evaluated by en face immunofluorescence and scanning electron microscope analyses of the fibrosa surface. Red blood cell (RBC) preparations were used in vitro to assess, by immunofluorescence microscopy and Alizarin red staining, the potential impact of intraleaflet hematomas on phenotypic changes in VIC.
Results: Intraleaflet hematomas, revealed by iron deposits and RBC into the fibrosa, secondary to endothelial micro-fissuring, were consistently found in non-calcified valves. The contact of primary VIC derived from these valves with RBC resulted in a global inflammatory and osteoblastic phenotype, reflected by the upregulation of IL6, IL1β, BSP, OPG, RANK, BMP2 and MSX2, the production of osteocalcin, and the formation of calcium deposits.
Conclusions: The acquisition of an osteoblastic phenotype in VIC that come into contact with the senescent RBC of intraleaflet hematomas may play a critical role in the initiation of calcium deposition into the *fibrosa* of human aortic valves.

CONDENSED ABSTRACT: Intraleaflet hematomas, revealed by ferric iron deposition, were found in whole-mount calcified and non-calcified human aortic valves. The presence of free iron in “healthy valves” may represent one of the earliest triggers leading to calcium deposition in human aortic valves. The iron deposits, which were likely released from RBC that had penetrated into the *fibrosa*, may be a consequence of endothelial injury that we observed during the early stages of aortic valve calcification. RBC penetration through endothelial micro-fissuring may drive the acquisition of an osteoblastic phenotype by VIC and determine the site of calcium deposition on aortic valves.

Key words. aortic valve stenosis, calcification, iron, hematoma, endothelium

ABBREVIATIONS
AC: Aortic valve calcification
AS: Aortic valve stenosis
PBS: Phosphate-buffered saline
RBC: Red blood cells
VEC: Valvular endothelial cells
VIC: Valvular interstitial cells
CBFA1: Core-binding Factor alpha 1
RANK: Receptor activator of nuclear factor NF-κB
BSP: Bone sialoprotein
MSX2: Muscle segment homeobox 2
BMP2: Bone morphogenic protein 2

Introduction

Stenosis due to degenerative aortic valve calcification (AC) is the most frequent valvular heart disease in the western world, and its prevalence, along with its public health burden, is increasing (1,2). While several mechanisms and pathways involved in the progression of AC have been described (3–5), little is known about the nature of the endogenous stimuli that initiate and trigger the cascade leading to the calcification of aortic valve leaflets. In non-pathological conditions, aortic valve leaflets are avascular and fully covered by valvular endothelial cells (VEC) that protect the valvular interstitial cells (VIC), nested in deeper layers of the *fibrosa*, from the bloodstream and its components. Past studies have linked intraleaflet hemorrhage, supposedly originating from neovascularization in human degenerative aortic stenosis (AS), to a more rapid progression of AC (6, 7). Whether intraleaflet hemorrhages are a cause or a result of calcium deposition cannot be inferred from these studies since they were exclusively conducted on severely calcified valves at advanced stages of the disease. In addition, establishing the spatial relationship between calcium deposition and post-hemorrhagic hematomas requires an analysis of the whole valve structure, not merely the sections of valve leaflets as performed thus far. In the present study, we establish a novel whole-mount immunohistological method and use it to analyze human aortic valves taken at the earliest stages of calcification. We hypothesize that a weakened endothelial barrier exposed to extreme hemodynamic conditions may contribute to the formation of intraleaflet hematomas and that the subsequent contact between VIC and the infiltrated, rapidly senescent red blood cells (RBC) could represent an initial step toward valve vulnerability by promoting calcification within VIC.

Methods

Aortic valve collection

Aortic valves were collected (Biobank BRIF: BB-0033-00029) from 1) consecutive patients who underwent surgical aortic valve replacement for severe AS, enrolled in an ongoing prospective cohort GENERAC (NCT00647088), aiming to identify factors involved in AS occurrence and progression; 2) patients who underwent combined coronary bypass surgery and aortic valve replacement for moderate AS; and 3) patients with healthy, calcium-free aortic valve leaflets from patients who underwent aortic valve replacement for severe pure aortic regurgitation not related to degenerative aortic valve disease; and 4) from heart explants in the context of heart transplantation for ischemic or idiopathic dilated cardiomyopathy. The latter valves were used for evaluating the presence of endothelial micro-fissuring. In order to avoid artefactual injury of the sample, the entire heart was explanted at a supravalvular level and transported immediately to our laboratory. After extensive washes in saline, the excision of the valve was carefully performed under microscope guidance. All aortic valves were immediately examined following tissue dissection, before any conditioning, and classified according to the degree of AC, including no calcification, microscopic calcifications, or macroscopic calcifications. Valves were thereafter washed in phosphate-buffered saline (PBS) and fixed by paraformaldehyde (PFA).

Whole-mount Alizarin and Perls' blue staining of valves

The proximity of calcium deposits with hematomas was visualized through the capacity of RBC, the most abundant cells in the blood, to release iron, which was evaluated by Perls' staining as described previously (8). After washing with distilled water, fixed valves were stained with Perls' blue solution freshly prepared from a mixture of 2.5% potassium ferrocyanide, 0.25% hydrochloric acid, and 0.02% Triton X-100, for 90 min at room temperature. Valves were then washed with water and stained with freshly prepared 0.04%

Alizarin red solution. After 1 h of incubation, the solution was discarded, samples were extensively washed with distilled water, and the tissue was clarified. The valve clarification method was adapted from the clearing procedure described by Yamazaki Y et al. (9). Briefly, valves were dehydrated successively in 25%, 50%, 75%, and 100% aqueous tetrahydrofuran solutions for 10 min and then for another 10 min in tetrahydrofuran and a freshly prepared solution of benzyl alcohol and benzyl benzoate at a ratio of 1:2 (BABB) (vol:vol). To increase valve transparency, tissues were placed in a BABB solution for 5–10 min. Valves were examined in 3D under a transmitted light microscope. Quantification of calcium and iron deposits was performed on all valves of the collection according to a 5-grade classification: grade 0 corresponded to the absence of both microscopic and macroscopic deposits, grade 1 to the presence of microscopic stains only (<5%), grades 2, 3, 4 and 5 to the detection of macroscopic deposits of, respectively, < 10%, < 30%, < 50% and > 75% of the valve surface.

Whole-mount immunofluorescence staining

We used whole-mount multiple immunofluorescence confocal microscopy (10) to distinguish VEC, VIC, and RBC with lectin-rhodamine (Ulex Europaeus Agglutinin I, Vector laboratories, Burlingame, California), anti-human αSMA (monoclonal, mouse, clone 1A4, Thermo Fisher Scientific, Waltham, Massachusetts) and anti-human glycophorin A (monoclonal, rabbit, Abcam, clone EPR8200) antibodies, respectively. Tissues were fixed in PFA, washed in water and then dehydrated in methanol. After rehydration in TBST (50 mM Tris-HCl pH 7.4, 150 mM NaCl, 0.1% TritonX-100), tissues were incubated in a blocking solution containing 10% serum and then with primary antibodies and lectin-rhodamine diluted in blocking solution containing 5% DMSO for 3 days. After extensive washing with TBST, incubation with secondary antibodies anti-mouse AF488 and anti-rabbit AF647 (Abcam, Cambridge, UK) was

carried out using the same procedure. Images were taken by LSM 780 confocal microscopy (Zeiss, Oberkochen, Germany).

Scanning electron microscopy

Valves were fixed in PFA, post-fixed in 2% glutaraldehyde and dehydrated in graded ethanol solutions. Samples were air-dried at room temperature and mounted on aluminum stubs with double-stick tabs. Tissues were coated with 10 nm graphite and imaging was performed under high-vacuum conditions at 10 or 20 kV using a Philips Quanta FEG 250 scanning microscope (ThermoFisher Scientific).

VIC isolation and culture

Primary human VIC were prepared as described previously (11) from non-calcified aortic valves obtained from explanted hearts of patients undergoing heart transplantation. The valve leaflets were excised and washed in PBS containing a 1% antibiotic mixture (penicillin, streptomycin, and fungicide). The leaflets were placed in a type I collagenase solution (0.22 units/mg) for 3 h at 37°C. After digestion, a cell suspension was obtained by removing undigested tissue pieces with a 70 µm cell strainer. Cells were suspended in a complete smooth-muscle-cell basal 2 medium (PromoCell, Heidelberg, Germany) with 10% fetal bovine serum (FBS) and a 1% antibiotic mixture (ThermoFisher Scientific). VIC were seeded in tissue culture flasks in complete media and used for experiments or further subcultures until passage 4.

Preparation of collagen scaffolds for 3D VIC culture and stimulation

To mimic physiological conditions, VIC were cultured in 3D collagen scaffolds (12). Fresh collagen solutions were prepared by mixing 0.3 ml of 10X concentrated DMEM, 0.3 ml of 0.25 M $NaHCO_3$ buffer, 0.3 ml of FBS, 0.3 ml of antibiotic mixture, 0.12 ml of 0.1 M NaOH and 2.5 ml of rat type I collagen (3 mg/ml, Gibco). After polymerization of the collagen mixture,

primary cultured cells were seeded on collagen scaffolds at 30 000 to 50 000 cells per well and incubated for 2 days in complete medium prior to the addition of RBC. Immunohistochemical staining and calcium deposits were analyzed in the cell cultures on days 5 and 7, respectively. Alizarin red (2%) was used to visualize calcium deposits.

Immunohistochemistry

VIC were rinsed with PBS and fixed in PFA, washed with TBS (50 mM Tris-HCl, 0.9% NaCl, 0.05% Tween) and permeabilized with PBS, 0.05% Triton100X and 1% BSA-glycine. Anti-human osteocalcin (monoclonal, mouse, clone 190125, R&D System, Minneapolis, USA) and anti-human glycophorin A (GPA; monoclonal, rabbit, Abcam, clone EPR8200) antibodies were incubated overnight and detected using the appropriate secondary antibodies (goat anti-mouse coupled to AF488 and anti-rabbit coupled to rhodamine). DAPI and AF647-coupled phalloidin (Life Technologies) were used for counter staining. Slides were cover-mounted with Prolong Gold Antifade Reagent (Invitrogen), and images were captured on an Axiovert 200 M® inverted microscope (Zeiss, Marly le Roi, France).

Red blood cell preparation

RBC were prepared from human peripheral blood (13) collected from healthy volunteers in heparinized tubes. The pellet containing RBC was mixed (1:1) with a dextran solution (2% in Hank's balanced salt solution, HBSS) for 15 min, centrifuged and washed with HBSS. The resulting fresh RBC (f-RBC) served as controls. The senescence of RBC from the same donor was induced by suspending f-RBC in HBSS supplemented with 0.1% glucose and incubated at 37°C for 5 days. The capacity of phosphatidylserine exposed on cell membranes to bind annexin-V-FITC was assessed by flow cytometry. Senescent red blood cells (s-RBC) were washed before *in vitro* assay to limit the direct effect of free hemoglobin.

Gene expression

VIC were cultured for 24 or 48 h in the presence of f-RBC or s-RBC. Total RNA was extracted from cells using Trizol reagent (Invitrogen). Reverse transcription was performed on 20 ng of total RNA with a Superscript III cDNA synthesis kit (Life Technologies) to obtain the cDNA target. Real-time PCR was performed on the CFX 100 (Biorad) cycler using the primers listed in Table 1. The reaction volume was performed with 1 ng of cDNA of each sample, 250 nM of forward and reverse primers and the Syber-Green master mix (Biorad). The amplification program was performed as follows: 1 cycle: 50°C, 2 minutes; 1 cycle: 95°C, 15 minutes; 50 cycles: 95°C 40 seconds and 60°C 1 minute. The expression of the genes of interest was normalized by the expression of the housekeeping gene hypoxanthine-guanine phosphoribosyltranferase (HPRT) and the expression of VIC stimulated by f-RBC using the $2^{-\Delta\Delta CT}$ method (14).

Phagocytosis assay of RBC

RBC were labeled with Cell Tracker Violet (ThermoFisher Scientific) and incubated with VIC. After 24 h, unbound RBC were removed by washing, and cells were dissociated with trypsin. The cells were suspended in PFA and analyzed by flow cytometry (LSRII, BD Biosciences, USA).

Statistical analysis

Variables were expressed as the mean ± standard deviation (SD) or number (percent). Distribution of variables was assessed using the Shapiro-Wilk normality test. Comparisons were performed using the t-test, the $\chi 2$ test, Wilcoxon test or Fisher's exact test as appropriate. A p value < 0.05 was considered statistically significant. Statistical analyses were performed using JMP 10 software (SAS institute, Cary, North Carolina).

Results

Aortic valve collection characteristics

To obtain a global overview of the AC process, we collected aortic valves from patients with severe and moderate AS as well as from patients free from any aortic valve disease. The valves were obtained from 40 (63%) patients with severe AS, 5 (8%) patients with moderate AS, 14 (22%) patients with pure aortic regurgitation, and 5 (8%) patients with healthy, calcium-free aortic valves from heart explants following heart transplantation. Baseline clinical and aortic valve characteristics in the overall population and according to the degree of AC are reported in Table 2. Briefly, the mean age of the patients was 66 ± 15 years, 43 (67%) were male, and the aortic valve mean pressure gradient was 42 ± 22 mmHg. Based on Alizarin red staining, 11 (17%) valves were calcium free, 18 (28%) had microscopic calcifications, and 35 (55%) had macroscopic calcifications.

Intraleaflet hematomas, detected by iron accumulation, precede calcium deposition

To establish a spatial link between calcium deposits and the areas of intraleaflet RBC accumulation, whole-mount examination of all aortic valves was performed after staining with Alizarin red and Perls' blue. An increasing amount of iron deposits was observed along with the increased calcium deposition within the valve as shown in the representative image (Figure 1A), even in non-calcified valves, suggesting that intraleaflet hematomas at the sites of valve calcification precedes the formation of calcium deposits. The quantified results for all 64 valves are presented in **Figure 1B**, confirming this observation.

Observation of valves with macroscopic calcifications collected from patients with severe AS revealed RBC accumulation in the immediate vicinity of the calcifications, mostly in areas adjacent to neo-angiogenesis (**Figure 2A**). Examination of valve leaflets obtained from

explanted hearts revealed the presence of iron deposits in the proximity of clusters of micro-calcification but without associated neovascularization (**Figure 2B**). In light of these findings, we hypothesized that the iron deposits during the early stages of AC may be a consequence of the penetration of RBC through VEC. Given that the endothelial layer is impermeable to RBC under physiological conditions, these observations suggested that the observed intraleaflet hematomas could be secondary to local breaching of the endothelial barrier. The penetration of RBC through breaches of the VEC layer could constitute the hematoma-forming mechanism dominating the early phase of AC, whereas hemorrhages through the leaky intra-valve neovessels, suggested by previous reports (6, 7), likely constitute an additional source of hematomas during advanced stages of AC.

Aortic valve endothelium injury is associated with intraleaflet RBC accumulation

To look for the presence of endothelial injury during the early stages of calcification, we analyzed the surface of the *fibrosa* side of the calcium-free valves by using scanning electron microscopy. We found areas of endothelial denudation in all valves, even in the absence of calcification (**Figure 3A, 3C, 3E and 3G**). Within these areas, RBC were entrapped in the matrix of the *fibrosa* (**Figure 3B, 3D, 3F and 3H**). To confirm these results, whole-mount immunostaining of VIC, VEC, and RBC, with, respectively, anti-αSMA, anti-lectin and anti-GPA antibodies, was performed on clarified aortic valves with microscopic calcifications and without neovascularization (**Figure 4**). Healthy areas contained VIC within the *fibrosa* covered by an unaltered endothelial barrier composed of VEC. In contrast, areas of endothelial denudation were characterized by a complete loss of VEC (**Figure 4A and 4B**). This loss of endothelium led to extensive penetration of RBC into the *fibrosa*, as revealed by confocal Z-series images of whole-mount valves (**Figure 4B**). Quantification of the mean fluorescence

intensity (MFI) revealed a decrease in VEC density leading to contact between RBC and VIC (**Figure 4C**). These results suggested that endothelial injury observed during early stages of calcification led to the deposition of iron that likely was released from RBC that had penetrated into the *fibrosa*.

Senescent RBC promote the differentiation of VIC toward an osteoblastic phenotype

Valve injury causes the infiltration of blood and the contact of its elements with the cells of the *fibrosa*, which is not a physiological condition. To mimic the biology of tissue-infiltrated blood *in vitro*, we used RBC prepared from healthy donors. The absence of leukocytes in these blood preparations allowed us to use them with VIC derived from a different donor. Furthermore, considering that the RBC undergo accelerated senescence after their accumulation in hematomas due to the static and pro-oxidative conditions (15,16), we prepared two types of RBC, senescent and fresh, to be used in our *in vitro* experiments with the VIC. We found that osteocalcin production and calcium deposits were observed only when VICs were co-cultured with senescent RBC (**Figure 5A**). Furthermore, VIC were able to acquire inflammatory and pro-osteogenic profiles when they were co-cultured with senescent RBC for 24 or 48 h, as shown in **Figure 5B**. A statistically significant increase in the expression of interleukin (IL) 6, IL1β, bone sialoprotein (BSP), osteoprotegerin (OPG), the receptor activator of nuclear factor NF-κB (RANK), bone morphogenic protein (BMP2) and the muscle segment homeobox 2 (MSX2).

Incubation of senescent RBC on collagen scaffolds in the absence of VIC did not lead to calcium formation, demonstrating the absolute requirement of VIC for calcification and excluding the possibility that an eventual interaction between the senescent RBC and the collagen scaffold could trigger calcification (online Figure 1). Interestingly, VIC were able to phagocytize senescent RBC, as shown by a representative orthogonal view using confocal

microscopy (Online Figure 2A). This result was confirmed by flow cytometry, which showed an increased incorporation rate into the VIC of senescent RBC loaded with a violet cell tracer (Online Figure 2B).

Discussion

The occurrence of intraleaflet hemorrhage has been recently suggested to accelerate the progression of human AC (6,7). These studies, however, exclusively focused on severely calcified valves at advanced disease stages. As a consequence, the etiopathogenic role of intraleaflet hematoma could not be evaluated.

In the present work, we analyzed a wide range of aortic valves in terms of calcification severity, including macroscopically and microscopically calcified valves representing early stages of the disease (**Central Illustration**).

Since the use of microscopic preparations does not allow for scanning for the presence of hematomas in the whole valve, we adopted a whole-mount method that allowed us to establish a precise spatial relationship between areas of hematoma and calcification. We observed that hematomas detected by ferric iron deposits could be found not only in calcified valves, as previously shown, but also in non-calcified valves, suggesting that intraleaflet hematomas may precede, and possibly initiate, the development of AC.

Indeed, iron and calcium are colocalized in the proximity of areas exposed to increased mechanical stress (18) and several lines of evidence point at the specific hemodynamic stress experienced by the aortic valve at each closing cycle as a potential initiating factor that could lead to AC (17). The *fibrosa* of aortic valve leaflets has a singular structure with circumferentially oriented collagen fibers (17, 19), and during the diastolic phase of the cardiac cycle, it is exposed to significant hemodynamic forces and abrupt deformation (17). These

hemodynamic and histological characteristics may contribute to the preferential occurrence of valve lesions within the fibrosa. We identified and quantified areas of endothelial denudation characterized by a complete loss of VEC and penetration of RBC from the blood stream into the fibrosa. This observation extends the previous paradigm by linking AC to intraleaflet hematomas not only due to the rupture of fragile neovessels observed during late stages of the disease but also to the extrinsic penetration of arterial blood into the fibrosa as a consequence of micro-fissuring at the earliest stages of AC. However, the micro-fissuring may not per se be considered a pathogenic trigger since all aortic valves are subjected to long-term mechanical stress. Thus, although the observed endothelial tearing may be considered an initiating event, other factors likely contribute to subsequent disease progression. In physiologic conditions, the minor injuries that may occur recurrently at the surface of the *fibrosa*, can be rapidly repaired by a highly coordinated series of events, including the activation of the blood clotting cascade, fibrin patch formation, and the inflammatory phase marked by the accumulation of neutrophils and macrophages, followed by a proliferative phase favoring tissue remodeling and reconstitution (20). In this sequence, the clearance of apoptotic cells, or efferocytosis, at the site of the lesion by macrophage engulfment constitutes a crucial step, as the persistence of apoptotic cells can impede wound healing (21, 22). Thus, accumulation of senescent RBC in areas of *fibrosa* micro-fissuring may witness a failure of the physiological efferocytosis, leading to a state of prolonged inflammation favoring the non-healing of wounds. In such a situation, blood could continue to leak through the damaged endothelial wall, and the resulting expansion of the unresorbed hematoma may amplify the pathologic loop by prolonging the contact with the blood elements and driving the observed osteoblastic phenotypic changes of the VIC.

Differentiation of VIC toward an osteoblast-like phenotype is a well described phenomenon (3, 4, 23, 24), but the exact mechanisms and the nature of the endogenous factors that initiate these phenotypic changes still remain largely unknown. In healthy aortic valve leaflets, VIC are quiescent, with a fibroblast-like phenotype. In the present study, we found that VIC were able to acquire an osteoblast-like phenotype following contact with blood elements, particularly senescent RBC. The latter may act by releasing high amounts of iron, which may eventually drive the phenotypic changes of the stromal cells leading to the calcification process, as suggested by recent reports (25,26). Our observation, however also points at a novel function of the VIC, suggested by their ability to engulf intact RBC. This observation suggests that besides macrophages, VIC could also contribute to the efferocytosis that is necessary to detoxify the valve microenvironment upon the occurrence of an intraleaflet hematoma and may, therefore, play a key role in the healing process of *fibrosa* injuries, thus contributing, under physiological conditions, to homeostasis of the aortic valve.

The contact of VIC with the elements of the bloodstream may represent a new pathophysiological mechanism, which needs to be confirmed by future investigations, contributing to the initiation of AC. Interventions capable of preventing the extension of early intraleaflet hematomas and/or promoting their effective efferocytosis as well as physiological repair processes certainly represent a future axis of research to stop the progression of AC.

The main limitation of our study is that the temporal sequence of the evolution of AC was not performed on the same individual, but the longitudinal approach we adopted by studying a broad range of aortic valves at different stages of AC allowed us to apprehend the natural history of the disease.

Conclusions

Human AC is tightly linked to the penetration of blood elements into the valvular tissue. Injuries are likely to occur recurrently on valves because the valves are required to perform heavy mechanical work. Repair processes keep valves healthy, but concomitant noxious conditions can disturb the biology of resident cells and promote pathological conditions. Repeated aortic valve intraleaflet accumulation of senescent RBC consecutive to unhealed endothelial injury is such a noxious condition that may promote VIC differentiation toward an osteoblastic phenotype and favor calcium deposition leading to calcific AS.

CLINICAL PERSPECTIVES

Competency in Medical Knowledge: Iron released from erythrocytes that penetrate into the fibrosa of human heart valves may be a consequence of endothelial injury during the early stages of calcification.

Translational Outlook: Further studies are needed to assess the potential therapeutic role of anti-inflammatory drugs that interfere with IL1β or IL-6 signaling on the progression of calcific aortic stenosis.

References

1. Baumgartner H, Falk V, Bax JJ, et al. 2017 ESC/EACTS Guidelines for the management of valvular heart disease. Eur Heart J. 2017;38:2739–2791.

2. Nishimura RA, Otto CM, Bonow RO, et al. 2014 AHA/ACC guideline for the management of patients with valvular heart disease: a report of the American College of Cardiology/American Heart Association Task Force on Practice Guidelines. J Am Coll Cardiol. 2014;63:e57-185.

3. Lindman BR, Clavel M-A, Mathieu P, et al. Calcific aortic stenosis. Nat. Rev. Dis. Primer 2016;2:16006.

4. Pawade TA, Newby DE, Dweck MR. Calcification in Aortic Stenosis: The Skeleton Key. J. Am Coll Cardiol. 2015;66:561–577.

5. Yutzey KE, Demer LL, Body SC, et al. Calcific aortic valve disease: a consensus summary from the Alliance of Investigators on Calcific Aortic Valve Disease. Arterioscler Thromb Vasc Biol. 2014;34:2387–2393.

6. Akahori H, Tsujino T, Naito Y, et al. Intraleaflet haemorrhage is associated with rapid progression of degenerative aortic valve stenosis. Eur Heart J. 2011;32:888–896.

7. Akahori H, Tsujino T, Naito Y, et al. Intraleaflet haemorrhage as a mechanism of rapid progression of stenosis in bicuspid aortic valve. Int J Cardiol. 2013;167:514–518.

8. Asleh R, Guetta J, Kalet-Litman S, Miller-Lotan R, Levy AP. Haptoglobin genotype- and diabetes-dependent differences in iron-mediated oxidative stress in vitro and in vivo. Circ. Res. 2005;96:435–441.

9. Yamazaki Y, Yuguchi M, Kubota S, Isokawa K. Whole-mount bone and cartilage staining of chick embryos with minimal decalcification. Biotech. Histochem. Off. Publ. Biol. Stain Comm. 2011;86:351–358.

10. Alanentalo T, Asayesh A, Morrison H, et al. Tomographic molecular imaging and 3D quantification within adult mouse organs. Nat. Methods 2007;4:31–33.

11. Chen J-H, Yip CYY, Sone ED, Simmons CA. Identification and characterization of aortic valve mesenchymal progenitor cells with robust osteogenic calcification potential. Am. J. Pathol. 2009;174:1109–1119.

12. Bellows CG, Melcher AH, Aubin JE. Contraction and organization of collagen gels by cells cultured from periodontal ligament, gingiva and bone suggest functional differences between cell types. J. Cell Sci. 1981;50:299–314.

13. Kolb S, Vranckx R, Huisse M-G, Michel J-B, Meilhac O. The phosphatidylserine receptor mediates phagocytosis by vascular smooth muscle cells. J. Pathol. 2007;212:249–259.

14. Pfaffl MW. A new mathematical model for relative quantification in real-time RT-PCR. Nucleic Acids Res. 2001;29:e45.

15. Minetti M, Agati L, Malorni W. The microenvironment can shift erythrocytes from a friendly to a harmful behavior: Pathogenetic implications for vascular diseases. Cardiovasc. Res. 2007;75:21–28.

16. Comporti M, Signorini C, Buonocore G, Ciccoli L. Iron release, oxidative stress and erythrocyte ageing. Free Radic. Biol. Med. 2002;32:568–576.

17. Bäck M, Gasser TC, Michel J-B, Caligiuri G. Biomechanical factors in the biology of aortic wall and aortic valve diseases. Cardiovasc. Res. 2013;99:232–241.

18. Thubrikar MJ, Aouad J, Nolan SP. Patterns of calcific deposits in operatively excised stenotic or purely regurgitant aortic valves and their relation to mechanical stress. Am. J. Cardiol. 1986;58:304–308.

19. Stella JA, Sacks MS. On the Biaxial Mechanical Properties of the Layers of the Aortic Valve

Leaflet. J. Biomech. Eng. 2007;129:757–766.

20. Eming SA, Krieg T, Davidson JM. Inflammation in wound repair: molecular and cellular mechanisms. J. Invest. Dermatol. 2007;127:514–525.

21. Gurtner GC, Werner S, Barrandon Y, Longaker MT. Wound repair and regeneration. Nature 2008;453:314–321.

22. Jun J-I, Kim K-H, Lau LF. The matricellular protein CCN1 mediates neutrophil efferocytosis in cutaneous wound healing. Nat. Commun. 2015;6:7386.

23. Mohler ER, Gannon F, Reynolds C, Zimmerman R, Keane MG, Kaplan FS. Bone formation and inflammation in cardiac valves. Circulation 2001;103:1522–1528.

24. Rajamannan NM, Evans FJ, Aikawa E, et al. Calcific aortic valve disease: not simply a degenerative process: A review and agenda for research from the National Heart and Lung and Blood Institute Aortic Stenosis Working Group. Executive summary: Calcific aortic valve disease-2011 update. Circulation 2011;124:1783–1791.

25. Laguna-Fernandez A, Carracedo M, Jeanson G, et al. Iron alters valvular interstitial cell function and is associated with calcification in aortic stenosis. Eur. Heart J. 2016;37:3532–3535.

26. Kawada S, Nagasawa Y, Kawabe M, et al. Iron-induced calcification in human aortic vascular smooth muscle cells through interleukin-24 (IL-24), with/without TNF-alpha. - PubMed - NCBI. Sci. Rep. 2018;8:658.

Figure Legends

Central Illustration: Intraleaflet Hematoma Promotes Aortic Valve Calcification. Blood penetration through an endothelial micro-fissure may drive the acquisition of an osteoblastic phenotype by VIC and determine the site of calcium deposition in human aortic valves. Endothelial micro-fissuring that occurs secondary to local hemodynamic stress allows RBC to penetrate into the fibrosa. The observation of free iron in "healthy valves" suggests that this could be the earliest trigger of the complex and chronic inflammatory process that leads to calcium deposition in aortic valves. In patients, the putative pathogenetic role played by such intraleaflet hematomas depends on the inability of VIC to cope with the entry of blood elements. Our *in vitro* data suggest that the initiation of calcium deposition in human aortic valves is driven by VIC that acquire an osteoblastic phenotype after coming into contact with infiltrated RBC displaying accelerated senescence and releasing free iron via RBC hemolysis. s-RBC: senescent red blood cell, VEC: valvular endothelial cells, VIC: valvular interstitial cells.

Figure 1. Intraleaflet iron accumulation precedes calcium deposition. A: Visualization of iron and calcium deposits on a representative whole-mount of clarified human valves with and without calcification. Whole-mount valves were imaged before (right) and after (left) Alizarin red and Perls' blue staining. The valves were optically cleared and observed 3-dimensionally under a transmitted light microscope. B: Quantification of calcium and iron within 11 calcium-free valves, 18 valves with microscopic calcifications, and 35 valves with macroscopic calcifications. An increasing amount of iron deposits along with increased calcium deposition was observed even in non-calcified valves, suggesting that RBC accumulation precedes the formation of calcium deposits.

Figure 2. Iron deposits are observed during the early stages of calcification in the absence of neovascularization. Whole-mount staining of clarified valves after Alizarin red and Perls' blue staining, showing hematomas in a calcified aortic valve and not in a calcium-free valve. A: Calcified valve obtained from a patient who underwent aortic valve replacement. Arrows indicate areas with neovascularization and hemorrhage close to calcium and iron deposits. B: Calcium-free valve obtained from an explanted heart showing iron deposits and limited areas of calcification without neovascularization (white arrow).

Figure 3. Early aortic valve endothelium injury leads to intraleaflet red blood cell accumulation. Scanning electron microscope views of the *fibrosa* side of human aortic valves from explanted heart without calcification (A, C, E, G). A: Area of the valve leaflet without endothelium injury. B: Zoomed view of the boxed area presented in A. C, E, G: Valve leaflet with endothelium denudation and penetration of RBC into the deeper layer of the *fibrosa*. D, E, F: Zoomed view of the boxed area presented, respectively, in C, E and G. RBC entrapped in the tissue (white arrows).

Figure 4. Endothelium injury allows early accumulation of RBC within the valve. A representative immunostaining with anti-αSMA (blue), lectin (green) and anti-GPA (red) in whole-mount staining of the entire clarified human valve reveals the loss of VEC and the possible contact between RBC and VIC (B). Quantification of mean fluorescence intensity (MFI) extracted from the area showed in B, revealing decreased VEC and increased RBC signals (C). Images A and B were taken with a 40× and a 63× objective lens, respectively, using the confocal Z-series microscope.

Figure 5. Senescent RBC promote valvular interstitial cell differentiation toward an osteoblastic profile *in vitro*. A: Human VIC were cultured on a scaffold collagen in the absence

(no RBC) or presence of 2×10^6 of fresh (f-RBC) or senescent (s-RBC) RBC. At day 5, immunofluorescent staining of the nuclei (DAPI), the actin cytoskeleton (phalloidin), osteocalcin (anti-osteocalcin) and RBC (anti-GPA) was performed in fixed cells. Cells cultured in the same condition were stained at day 7 by Alizarin red to visualize calcium deposits. B: The expression levels of IL6, IL1β, CBFA1, BSP, OPG, RANK, BMP2 and MSX2 were determined by RT-QPCR on RNA extracted from VIC co-cultured with f-RBC or s-RBC for 24 or 48 h. The gene expressions were determined by reverse transcription quantitative polymerase chain reaction (RT-qPCR) and analyzed using the $2^{-\Delta\Delta Ct}$ Pfaffl formula (14), in which data were normalized to the expression of VIC stimulated with f-RBC at 24 h and to the values of hypoxanthine-guanine phosphoribosyltransferase (HPRT). Data are representative of four independent experiments. Results are presented as the mean ± SEM and were analyzed with paired t-tests : *$p<0.05$; **$p<0.01$; ***$p<0.0001$.

Table 1. Human primers used for quantitative real-time PCR

Gene	Forward	Reverse
HPRT	TGAGGATTTGGAAAGGGTGT	GAGCACACAGAGGGCTACAA
IL6	GAAAGCAGCAAAGAGGCA	GTATACCTCAAACTCCAA
IL1β	CGAATCTCCGACCACCACTA	GATCGTACAGGTGCATCGT
CBFA1	CCTCTGGCCTTCCACTCTCA	GACTGGCGGGGTGTAAGTAA
BSP	TCAGCATTTTGGGAATGG	TCTTCGGATGAGTCACTAC
OPG	GAAGCTGGAACCCCAGAG	GTGTTGCATTTCTGAGTTA
RANK	AGGGAAAGCACTCACAGCTAA	ACATGCTCCCTGCTGACC
BMP2	AACGGACATTCGGTCCTTGC	CCATGGTCGACCTTTAGGAGA
MSX2	CCTGTTGAGAGGAATTGATGG	AAAGGTATACCGGAGGGAGG

Table 2. Baseline clinical and aortic valve characteristics in the overall population and according to degree of calcification

	Overall population (N = 64)	No calcification (N = 11)	Microscopic calcification (N = 18)	Macroscopic calcification (N = 35)	p
Age (years)	66 ± 15	47 ± 12	70 ± 15	72 ± 9	< 0.0001
Men	43 (67)	9 (82)	11 (61)	23 (66)	0.47
Coronary artery disease	18 (28)	2 (18)	6 (33)	10 (29)	0.66
Diabetes	14 (22)	2 (18)	3 (17)	9 (26)	0.71
Hypertension	28 (44)	3 (27)	7 (39)	18 (51)	0.33
Hypercholesterolemia	22 (34)	1 (9)	4 (22)	17 (49)	< 0.02
Smoking	24 (38)	5 (46)	8 (44)	11 (31)	0.54
Anticoagulation therapy	12 (19)	4 (36)	4 (22)	4 (11)	0.17
Antiplatelet therapy	18 (29)	2 (18)	5 (28)	11 (31)	0.68
Mean pressure gradient (mmHg)	42 ± 22	7 ± 9	36 ± 8	51 ± 16	< 0.008

Data are expressed as the mean ± SD, or number (percentage)

Figure 1

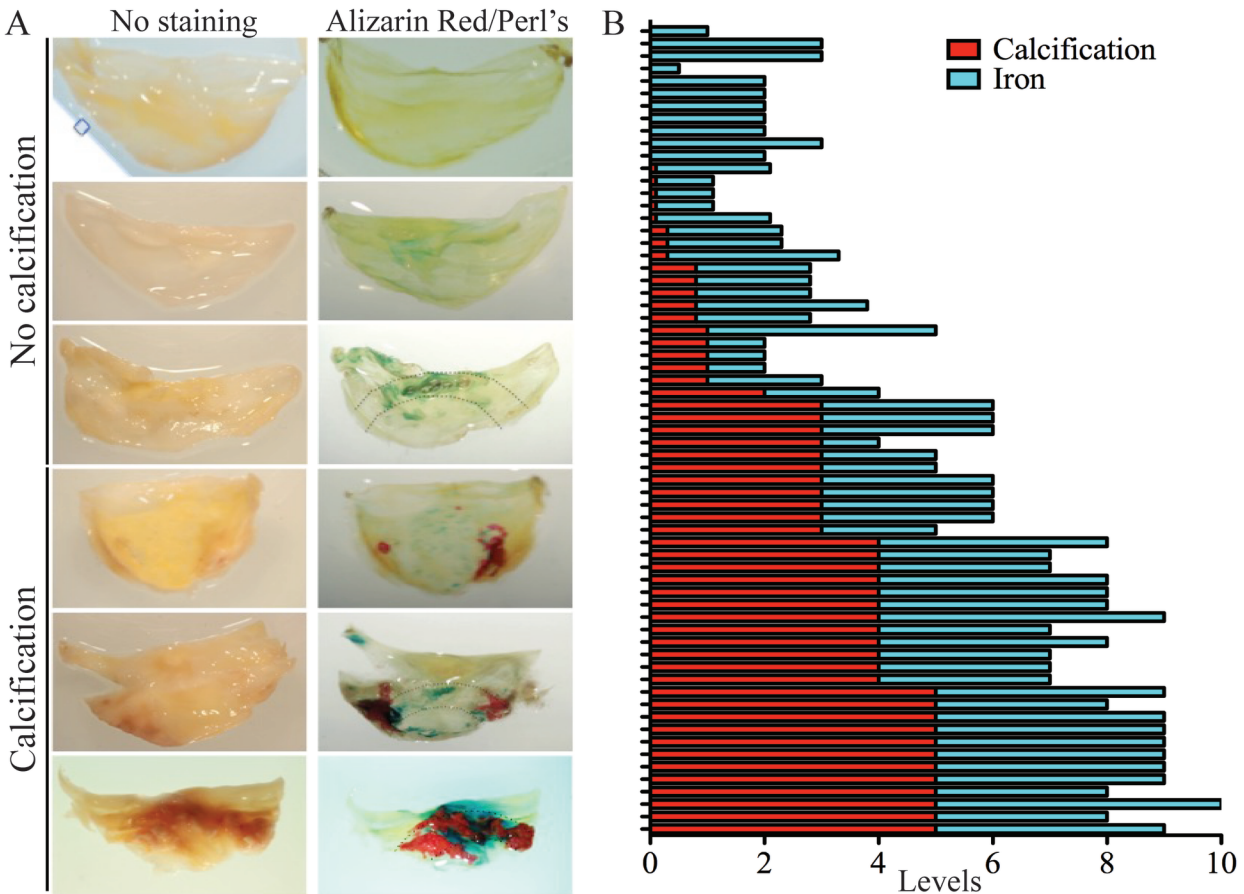
A
No staining
Alizarin Red/Perl's
No calcification
Calcification
B
Calcification
Iron
0
2
4
6
8
10
Levels

Figure 2

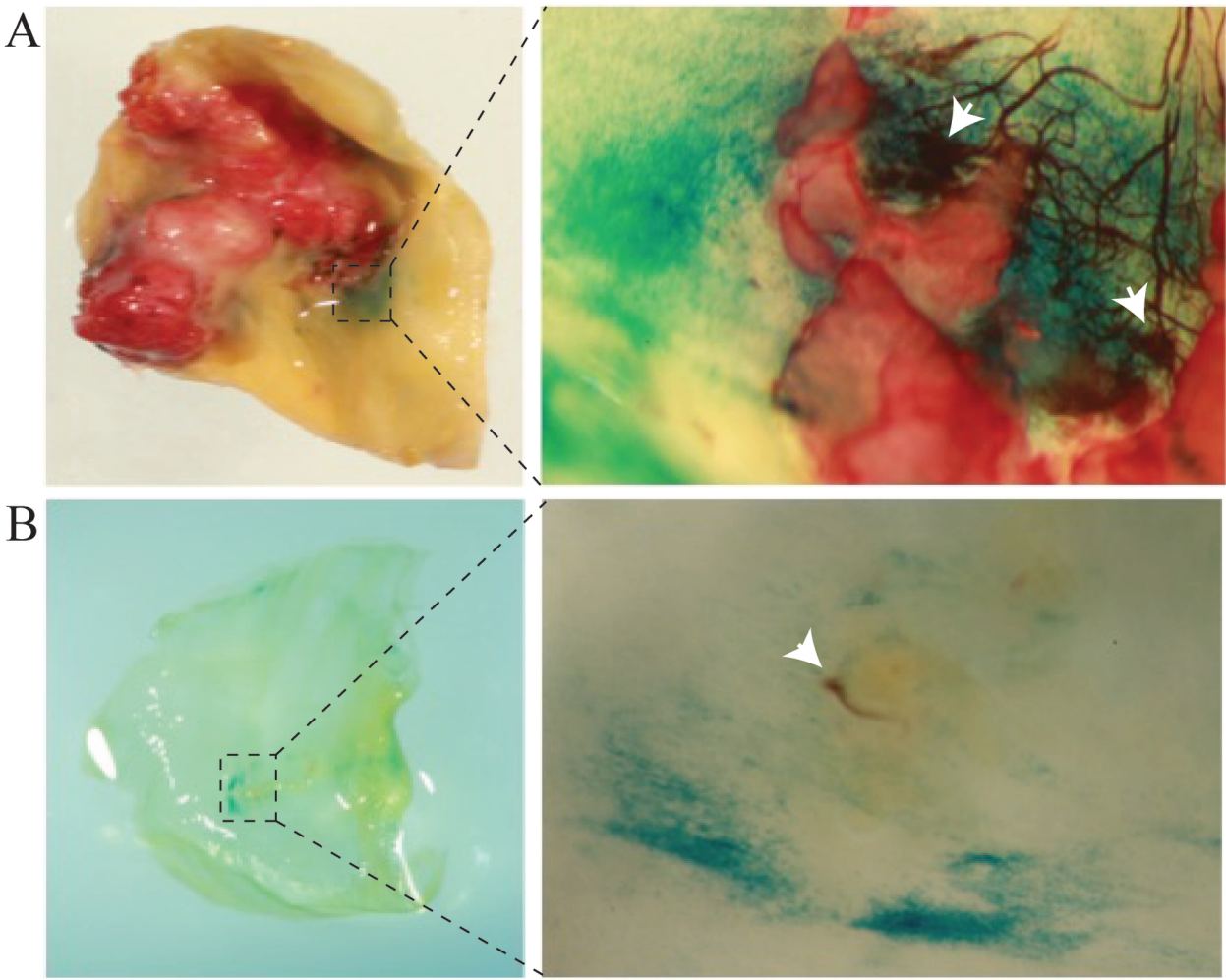

Figure 3

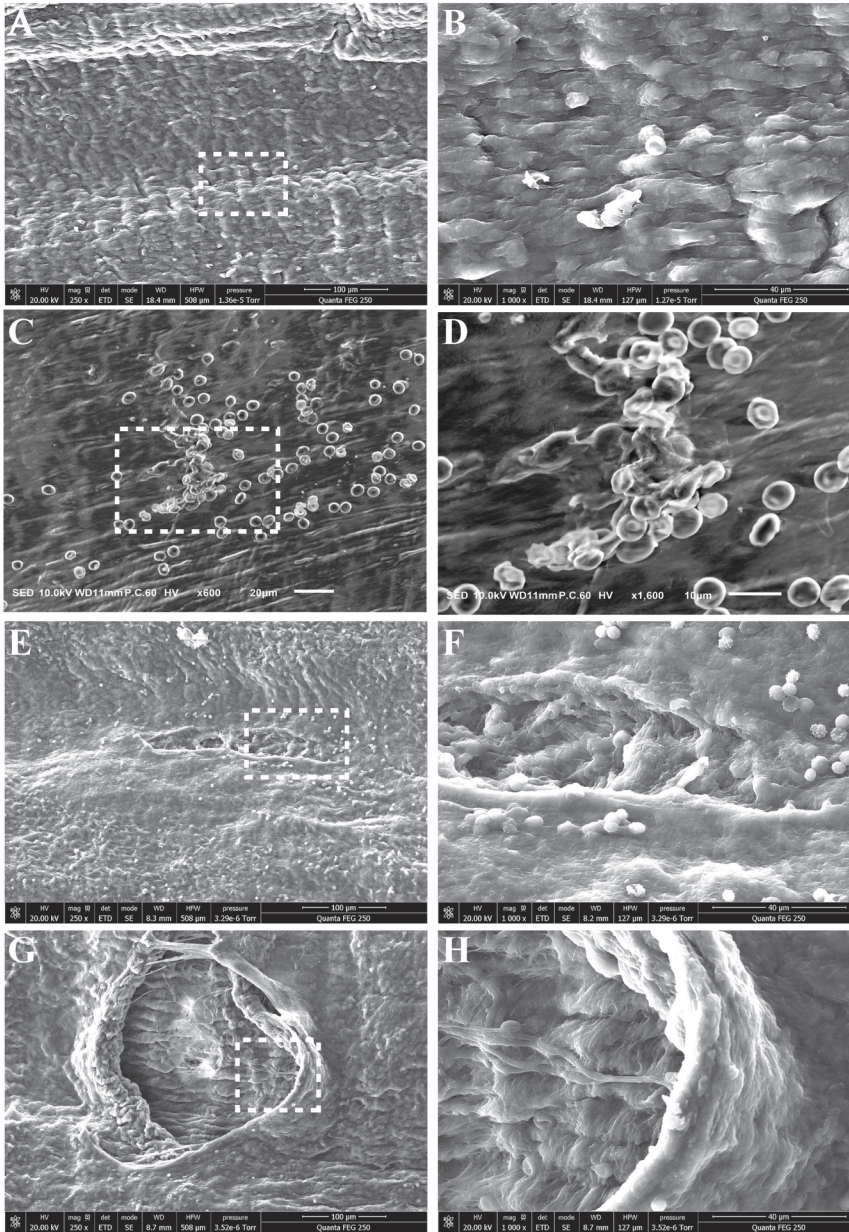
A
B
C
D
E
F
G
H
SED 10.0kV WD11mm P.C.60 HV x600 20µm
SED 10.0kV WD11mm P.C.60 HV x1,600 10µm
Quanta FEG 250

Figure 4

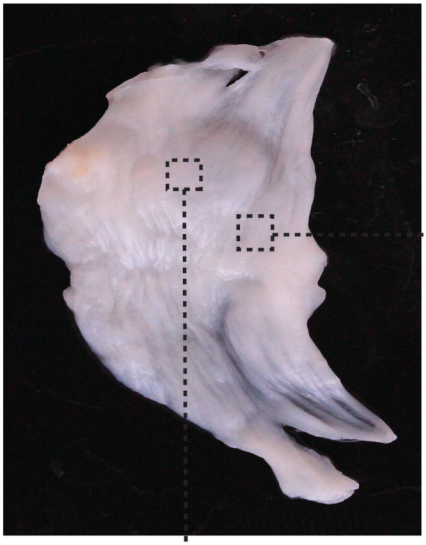

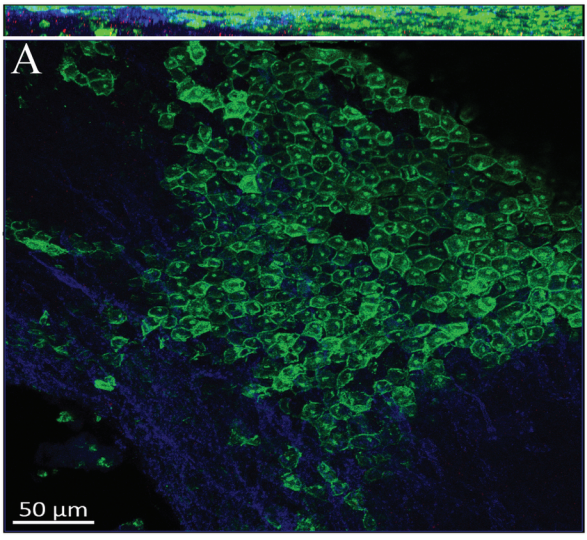
A
50 µm

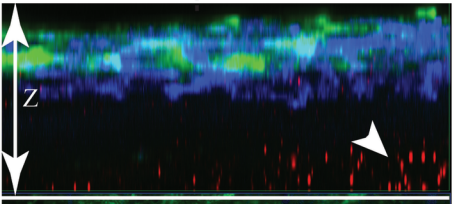
z

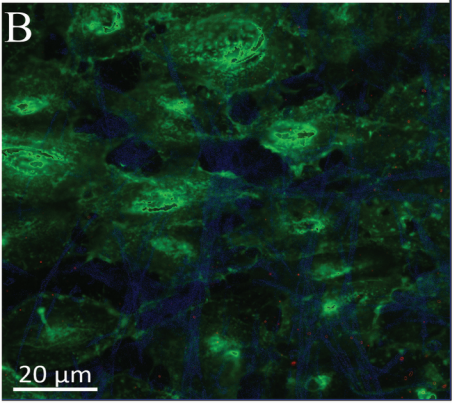
B
20 µm

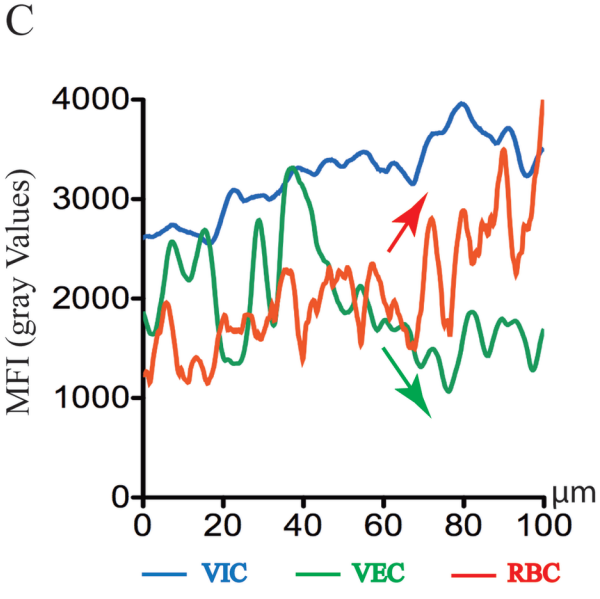
C
MFI (gray Values)
4000
3000
2000
1000
0
µm
0
20
40
60
80
100
VIC
VEC
RBC

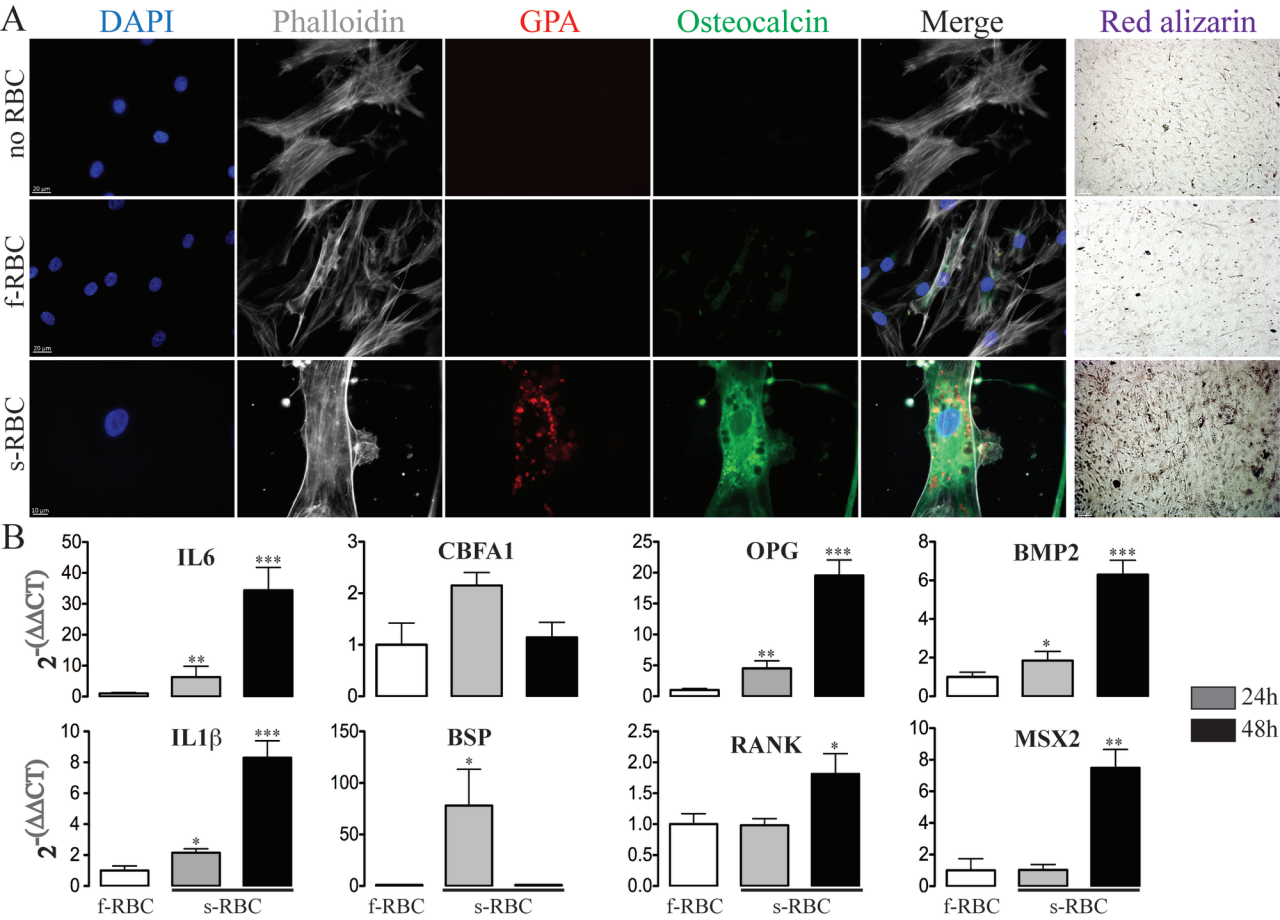
A
DAPI
Phalloidin
GPA
Osteocalcin
Merge
Red alizarin
no RBC
f-RBC
s-RBC
B
IL6
CBFA1
OPG
BMP2
IL1β
BSP
RANK
MSX2
2-(ΔΔCT)
24h
48h
f-RBC
s-RBC